

Reversible Redox-Driven Crystallization in a Paracyclophane Monolayer at a Solid–Liquid Interface

Zhi Li, Kunal Mali, Philippe Hapiot, Steven De Feyter, André-Jean Attias,*
and Stijn F. L. Mertens*

The development and integration of cyclophanes into future functional materials require a detailed understanding of the physicochemical principles that underlie their properties, phase behavior, and in particular the relationship between structure and function. Here, electrochemically switchable crystallization of a ferrocene-bearing 3D Janus tecton (M-Fc) at the interface between highly oriented pyrolytic graphite (HOPG) and an electrolyte solution is demonstrated. The M-Fc adlayer is successfully visualized under both ambient and electrochemical conditions using scanning tunneling microscopy. Voltammetric measurements show a surface-confined redox process for the M-Fc modified surface that drives the phase transition between a visible 2D ordered linear phase (M-Fc⁰, with ferrocene in the neutral state) and an invisible gas-like adsorption layer with high mobility when ferrocene is oxidized, M-Fc⁺, and a “square scheme” mechanism explains the data. Analogous experiments in a ferrocene-free tecton adlayer show no phase transition and confirm that the dynamics in M-Fc are redox-driven. On-surface 3D nanoarchitectures are also demonstrated by forming inclusion complexes between M-Fc and β -cyclodextrin and device behavior through electrochemical scanning tunneling spectroscopy (STS). These results showcase the functional potential of this class of cyclophanes, which can find use in actuators, optical crystals, and other smart materials.

due to their unique topology. Consisting initially of two benzene rings rigidly held in a face-to-face position by methylene bridges in the para positions, a wide range of designs have been developed to date, that generally comprise two aromatic subunits, and even polycyclic aromatic systems, connected in a face-to-face orientation through spacers.^[3] The resulting interactions between the two co-facial π -electron systems lead to unique structural, optical, and electronic properties which have been intensively studied over the past decades in view of applications that include asymmetric catalysis,^[4] organic electronics and photonics,^[5] and molecular machines.^[6] More recently, cyclophanes have emerged in nanoscience for the “bottom-up” fabrication of molecular electronic components by using them as 3D double decker units when adsorbed at metal surfaces.^[7] These specifically designed cyclophanes consist of two rigidly separated π -conjugated systems, one of which adsorbs on the metal substrate while the other is lifted above it, providing its electronic decoupling from the metal surface. The archetypal molecule is a naphthalenediimide cyclophane (NDIC),^[8] for which the electronic decoupling of the upper deck was demonstrated by scanning tunneling spectroscopy (STS),^[7b] and scanning tunneling microscope

1. Introduction

Since the first synthesis of “di-*p*-xylene” by Brown and Farthing in 1949^[1] and a series of [2.2]paracyclophanes by Cram and Steinberg in 1951,^[2] cyclophanes have attracted tremendous interest

Z. Li, K. Mali, S. De Feyter, S. F. L. Mertens
Department of Chemistry
KU Leuven
Celestijnenlaan 200F, Leuven 3001, Belgium
E-mail: s.mertens@lancaster.ac.uk

Z. Li
School of Chemical Engineering
Anhui Provincial Key Laboratory of Specialty Polymers
Anhui University of Science and Technology
Huainan 232001, China

 The ORCID identification number(s) for the author(s) of this article can be found under <https://doi.org/10.1002/adfm.202315861>

© 2024 The Authors. Advanced Functional Materials published by Wiley-VCH GmbH. This is an open access article under the terms of the [Creative Commons Attribution](#) License, which permits use, distribution and reproduction in any medium, provided the original work is properly cited.

DOI: 10.1002/adfm.202315861

P. Hapiot
Univ. Rennes
CNRS
ISCR – UMR 6226
Rennes F-35000, France
A.-J. Attias
Sorbonne Université
CNRS
MONARIS – UMR 8233
Paris F-75005, France
E-mail: andre-jean.attias@sorbonne-universite.fr
S. F. L. Mertens
Department of Chemistry
Energy Lancaster and Materials Science Lancaster
Lancaster University
Lancaster, Bailrigg LA1 4YB, United Kingdom

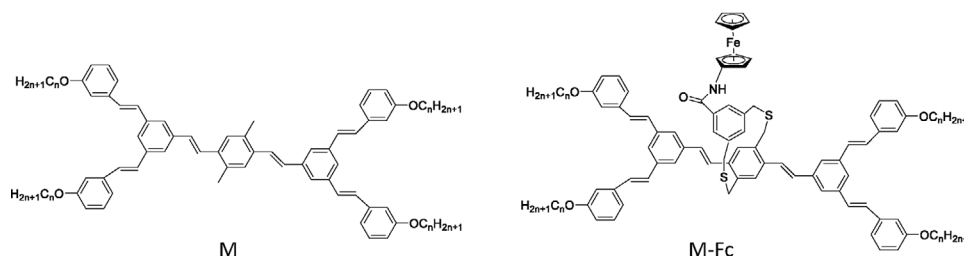


Figure 1. Chemical structure of molecular pedestal M and ferrocene-functionalized paracyclophane M-Fc.

(STM)-induced light emission was reported, but at low temperature and in ultrahigh vacuum.^[7c]

The next step, to go beyond these results obtained from discrete molecules adsorbed on a metal surface, consists in elaborating large-scale functional surfaces whose properties are induced by an assembly of molecules, under ambient conditions. With this aim, we previously developed a strategy combining 3D cyclophane-based building blocks (Janus tectons) to provide the functionality, and supramolecular self-assembly at surfaces to organize them in a well-defined 2D adlayer.^[9] A Janus tecton consists of two “faces” linked by a cyclophane, mostly [2.2]paracyclophane, where one face (pedestal) is responsible for the self-assembly on the surface and the second bears an active or “functional” component. The role of the cyclophane as linker is to act as a nanopillar when the molecule stands up on the surface, and thus spatially lifts the active component allowing its electronic decoupling from the metal surface.

A future vision of advanced self-assembled structures includes the bottom-up construction of strongly hierarchical structures, in two, three or four dimensions, that evolve and adapt to changing circumstances all the way up to nano- or mesoscale robots that can be programmed to perform sophisticated functions. An important aspect of such constructs will also be their reliable dis- and reassembly, for instance under the influence of an external stimulus (e.g., light, temperature, electric or magnetic field).^[10]

In this paper, we investigate a ferrocene-functionalized paracyclophane M-Fc, **Figure 1**, on highly oriented pyrolytic graphite (HOPG), and explore its molecular self-assembly, cyclic voltammetry and the possibility of structural switching under electrochemical conditions. The Fc moiety is covalently linked to a planar molecular pedestal moiety that facilitates its self-assembly on graphite. For reference, also the non-functionalized molecular pedestal M alone is investigated. In particular, we explore the question of whether a small change in a large molecule—the oxidation state of a single Fe ion, well removed from the surface—can lead to changes in the long-range order of an entire 2D crystal. Beyond electrochemical switching, toward further development of cyclophanes as multifunctional parts in a “supramolecular toolbox”, we investigate whether i) functionalization of the pedestal can be orthogonal to structural and functional behavior; ii) additional supramolecular principles and binding motifs that can give access to higher levels of structural complexity, such as the formation of host–guest complexes, are still fully operational, and iii) sophisticated electronic and other functions can be successfully built into cyclophane-based nanoarchitectures.

2. Results and Discussion

The self-assembly behavior of the molecular pedestal M and the ferrocene-functionalized 3D tecton M-Fc was investigated at the HOPG/1-phenyloctane interface using STM imaging. **Figure 2a,b** shows large-scale and high-resolution STM images of M, indicating that a linear structure is formed with the planar cores parallel to each other and the alkyl chains interdigitating. The molecular rows run along specific directions nearly parallel to one of the main symmetry axes of the HOPG substrate, as is typical for alkylated molecules on graphite.^[5f,g,9a] The unit cell of the packing is measured as $a = 3.80 \pm 0.20$ nm, $b = 2.18 \pm 0.20$ nm, $\gamma = 66 \pm 1^\circ$, with all values calibrated against the bare substrate. **Figure 2c,d** shows the equivalent images for the 3D tecton M-Fc and indicate a similar linear packing as for M, with unit cell parameters $a = 3.89 \pm 0.10$ nm, $b = 2.14 \pm 0.20$ nm, $\gamma = 68 \pm 1^\circ$. Comparing the large-scale images of M and M-Fc under identical tunneling conditions, **Figure 2a,c**, an additional bright protrusion is observed for M-Fc, which we attribute to the Fc functional group and its linker or nanopillar above the molecular pedestal M. In high-resolution imaging mode, **Figure 2b,d**, more blurring is apparent for M-Fc than for M, as larger local height differences are encountered by the STM tip, and a faster response of the feedback loop is required for accurate imaging.

To allow direct comparison of the two molecules under identical imaging conditions, and to study their mixing or segregation at the molecular level, also an equimolar mixture of M and M-Fc (each present at 1×10^{-6} M) was investigated by STM, **Figure 3**. Even though limited submolecular resolution is achieved, linear packings similar to the pure M and M-Fc adlayers are found. Importantly, no signs of molecular segregation are seen, as a random sequence of dark (M) and bright (M-Fc) features in each row is found, each adding up to 50% coverage. This randomness, and the parity of both molecules on the surface as in the supernatant, indicate that no preferential patterning (e.g., A-B-A-B...) occurs, that mixing of the two compounds happens at the molecular level, and that consequently, no significant thermodynamic or kinetic effects are associated with the presence of the cyclophane-based nanopillar and Fc group on the 2D crystallization of the molecular pedestal at the HOPG/phenyloctane interface. An intermediate conclusion, particularly important for the application of paracyclophane molecular building blocks, is that their synthetic modification can be orthogonal to their self-assembly properties.

Before conducting electrochemical measurements and EC-STM imaging, dry films of M and M-Fc were prepared, as phenyloctane and similar solvents are not compatible with

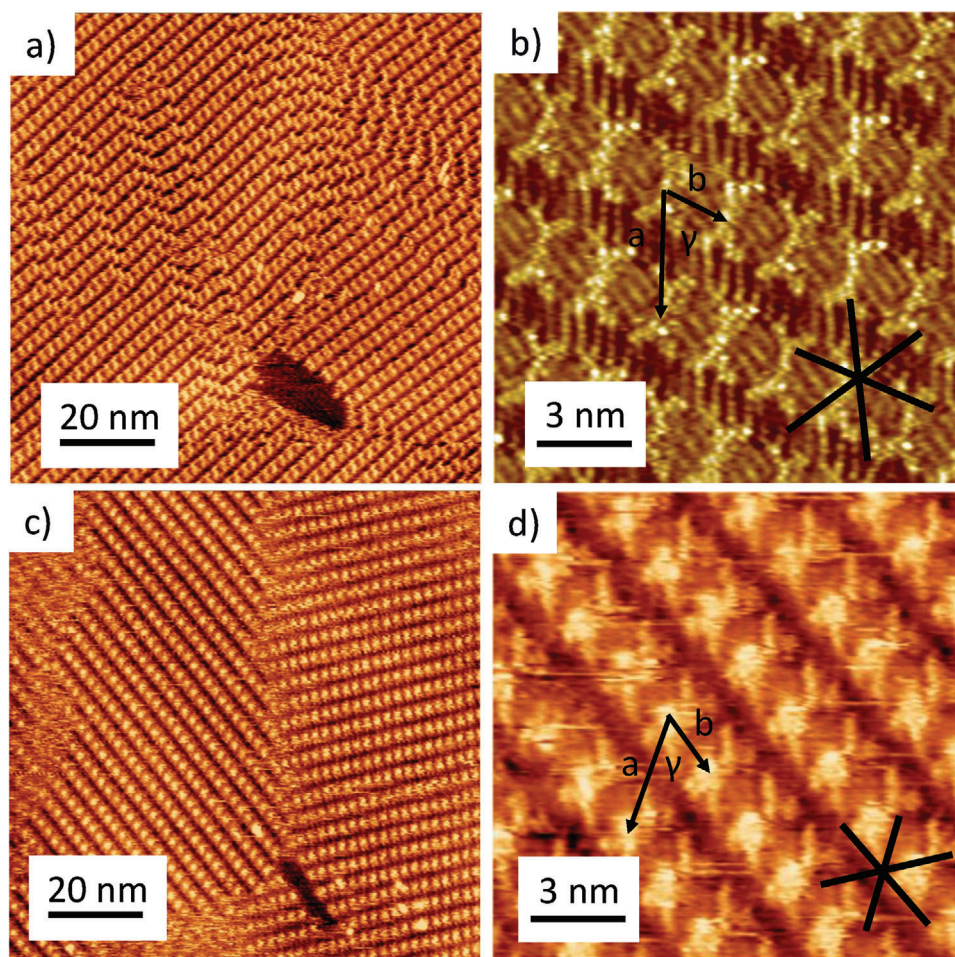


Figure 2. STM images of a,b) M and c,d) M-Fc at the HOPG/1-phenyloctane interface at a concentration of 2×10^{-6} M. Tunneling parameters: $V_{\text{bias}} = -0.5$ V and $I_t = 0.1$ nA.

electrochemistry. Saturated solutions in ethanol were diluted 100 times and drop-cast onto freshly cleaved HOPG substrates with slow evaporation of the solvent, followed by rinsing of the surface with 10 mL milli-Q water to remove any loosely bonded molecules or aggregates. **Figure 4** shows tapping mode AFM images of the drop-cast films in air, revealing high sur-

face coverage with multiple domains in orientations of multiples of 60 or 120°, again indicating the templating effect of the graphite substrate. The mirroring of dots in the Fast Fourier Transforms (FFT) of the images further indicates that the molecules can be arranged into left-handed and right-handed domains.^[5a,b]

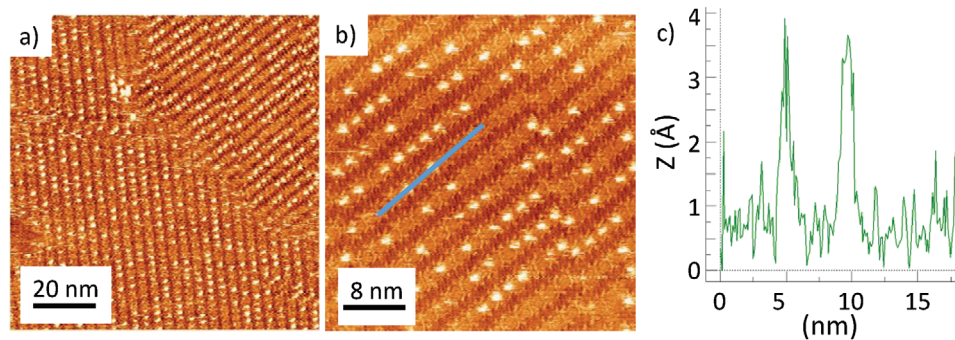


Figure 3. a,b) STM images of an equimolar M:M-Fc mixture (each 1×10^{-6} M in phenyloctane) on HOPG, and c) line profile along the blue trace in panel b). Tunneling parameters $V_{\text{bias}} = -0.5$ V and $I_t = 0.1$ nA.

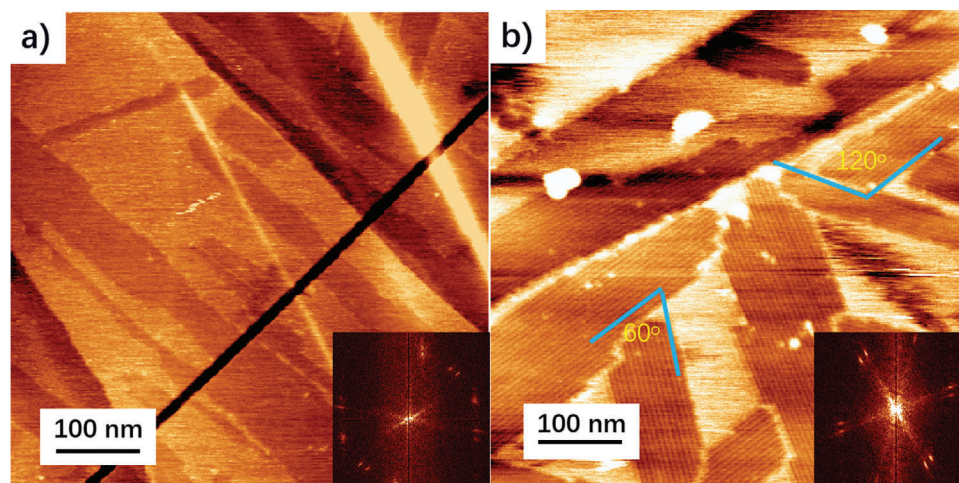


Figure 4. Tapping mode AFM height images of drop-cast films of a) M and b) M-Fc at the HOPG/air interface. Insets show corresponding FFT images.

We start the electrochemical study of the cyclophanes by considering the cyclic voltammogram (CV) of M-Fc in dichloromethane (DCM, a good solvent for M-Fc) containing 0.1 M Bu_4NPF_6 as supporting electrolyte and using HOPG as a working electrode, **Figure 5**, blue trace. Well-defined quasi-reversible redox behavior is observed, consisting of an oxidation peak for the neutral ferrocene and a reduction peak for the ferrocenium cation, with a formal potential of 0.35 V versus $\text{Ag}/\text{AgCl}/3\text{ M NaCl}$. No other redox features are apparent in the potential range between 0 and 1.2 V, even though anion intercalation has been described at higher potentials and may explain the current increase close to the positive limit.^[11]

Moving to the redox behavior of the drop-cast M-Fc film on HOPG in aqueous 0.1 M NaClO_4 , **Figure 5**, red trace, clear redox peaks are again visible, but are found 0.7 V more positive. This indicates that it is thermodynamically more difficult to oxidize the

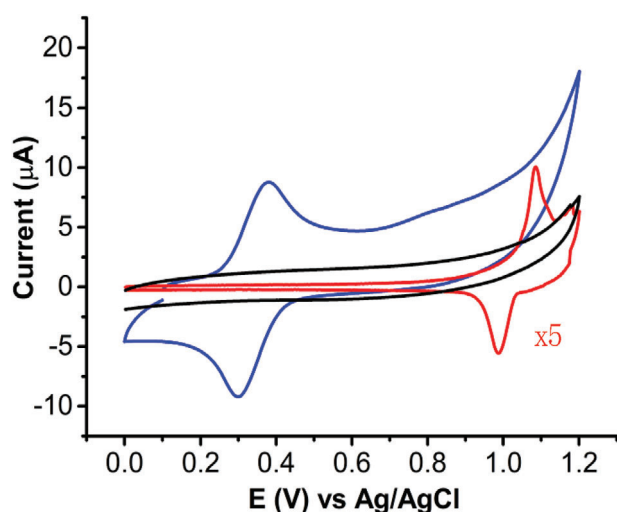


Figure 5. CVs of drop-cast M/HOPG (black trace) and M-Fc/HOPG (red trace) in 0.1 M NaClO_4 (aq), and of 5.76×10^{-4} M M-Fc + 0.1 M Bu_4NPF_6 dissolved in DCM at an HOPG electrode (blue trace). Scan rate, 100 mV s^{-1} . CE: Pt wire; RE: Ag/AgCl .

surface-confined M-Fc in an aqueous solution than freely diffusing M-Fc in DCM, which combines effects of electrostatics and hydrophobicity: on oxidation, counter ion association with the charged adlayer is necessary for electroneutrality reasons, and the close spacing in the adlayer makes this unfavorable. Finally, by contrast with M-Fc, M/HOPG shows no redox features, **Figure 5**, black trace. We note that the capacitive current is markedly larger for M/HOPG than for M-Fc/HOPG, reflecting the difference in height of the adlayer. In the double-layer charging region (0.0 to 0.9 V), a more compact adlayer (here, M) represents a thinner dielectric that separates the substrate from the electrolyte, leading to a higher interfacial capacitance.

The scan rate dependence of peak positions and currents in cyclic voltammetry is often used to distinguish between freely diffusing and surface-confined redox species.^[6,12] Peak currents proportional to the square root of the scan rate indicate redox species diffusing in solution, whereas peak currents proportional to the scan rate itself are indicative of a surface-bound redox species. The linear variation of the current with the square root of the scan rate in **Figure 6** confirms that M-Fc in DCM remains dissolved during cycling and that the current is controlled by the mass transfer from the solution to the electrode, ruling out strong adsorption.^[12a] Conversely, the roughly linear variation of peak current with scan rate for M-Fc/HOPG in aqueous perchlorate solution is indicative of a surface-bound electrochemical process during cycling, eliminating the possibility of collective desorption.^[13] Closer inspection of the rate-dependent CVs reveals several subtleties, however, both for the measurements in DCM and in aqueous perchlorate. For M-Fc in DCM, the peak position for the oxidation process is constant to within 10 mV for different scan rates, whereas the reduction peak shifts monotonously over 30 mV in the negative direction between the slowest and the fastest scan rate. This negative shift may indicate a kinetic barrier in dissociation of the ion pair $\text{M-Fc}^+ \text{PF}_6^-$ that is formed during oxidation in DCM with an intermediate dielectric constant of 8.93 at 298 K.^[14]

For the M-Fc/HOPG film in aqueous perchlorate, the discrepancies with the simplest behavior for immobilized redox species are stronger, and point at a more complex mechanism. First,

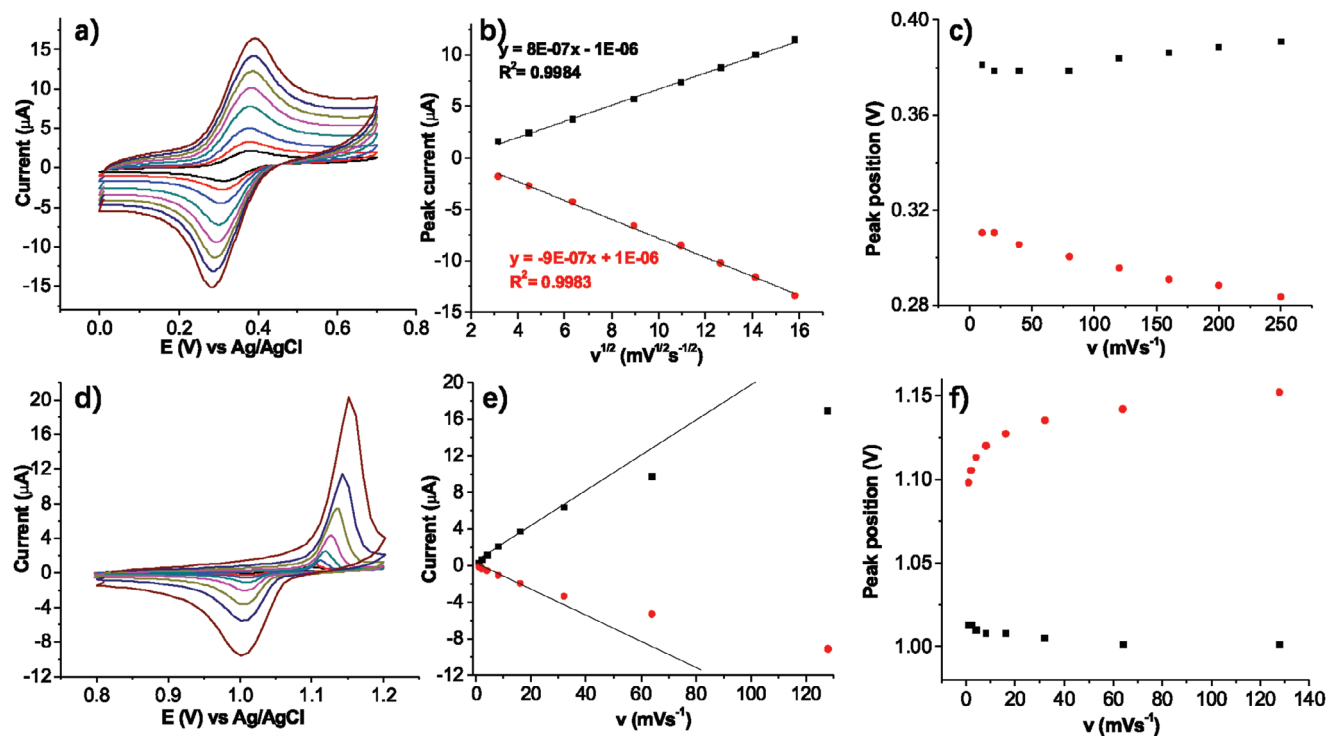


Figure 6. Scan rate dependent CVs of a,b,c) HOPG in 5.8×10^{-4} M M-Fc + 0.1 M Bu_4NPF_6 in DCM and d,e,f) M-Fc/HOPG in aqueous 0.1 M NaClO_4 . Scan rates were varied between 10 and 260 mV s^{-1} .

there is a significant separation between oxidation and reduction peaks, and its value increases first rapidly, then more slowly with scan rate, Figure 6f. Second, there is a strong asymmetry in peak shapes, which for any given scan rate are both higher and narrower for oxidation than for reduction. These features, and in particular the observed asymmetry between oxidation and reduction peak shapes, strongly suggest that a chemical (i.e., non-redox) step is part of the mechanism, which is absent for the freely diffusing M-Fc in DCM. Based on the electrochemical STM results we present in the next section, and on the simulation of the cyclic voltammogram, we will identify this chemical step as the equilibrium between M-Fc in a 2D crystal and in a 2D gas-like adsorption layer (vide infra).

Having established that M and M-Fc self-assemble at the solid-liquid interface, and that M-Fc has a clear redox signature originating from its ferrocene substituent, we now move to EC-STM measurements to explore any potential-dependent supramolecular effects. Phase transformations in molecular adlayers under electrochemical conditions have been studied extensively,^[15] but are not limited to redox molecules or even to electrolytic environments, as the electric field between tip and substrate in an STM can be used to confine collective responses at an electrode-electrolyte interface to the single-molecule level.^[16] Whereas potential-driven phase transitions have been mostly studied on metal substrates, the present work focuses on HOPG, a clearly underrepresented substrate in EC-STM.

The electrochemical behavior of the M-Fc/HOPG and M/HOPG in the EC-STM setup, Figure 7, retains the key features visible in Figure 5 in a standard cell, with a pair of redox peaks for M-Fc >100 mV apart and a featureless curve

for M, and allowing for the change in reference electrode. Figure 7b,c shows the self-assembled structures of M-Fc/HOPG at a substrate potential $E_s = 0.1$ V versus Pt, where the ferrocene group is in the reduced, uncharged state. The molecules are seen to pack in lamellar structures in the three main directions of the substrate, similar to our earlier observations at the phenyloctane/HOPG interface (Figure 2) and in dry films at the air/HOPG interface (Figure 4). Even though the resolution achieved in electrochemical environment is lower than in phenyloctane, the molecular rows and domain boundaries can be identified unambiguously. In higher-resolution images, Figure 7c, the width of a molecular row (≈ 3.8 nm) approaches the value found at the phenyloctane-HOPG interface, suggesting that essentially the same packing is present under electrochemical and non-electrochemical conditions. Similar observations are valid for M/HOPG, Figure 7e,f.

Figure 8 shows EC-STM images of the same sample area as a function of the substrate potential E_s , which is made progressively more positive. As E_s approaches the value required for oxidation of M-Fc/HOPG, the crystalline domains are seen to become smaller and to disappear when E_s reaches 0.4 V versus Pt. In view of the insolubility of M-Fc in aqueous solutions, we ascribe this observation to the formation of a 2D gas-like M-Fc⁺ adsorption layer, similar as postulated by Sagara et al. for dibenzylviologen.^[17] The high mobility of the molecules within the adlayer prevents their imaging with standard STM methods, and would require video rate STM.^[18] Taking this observation one step further, we set out to explore adlayer dynamics at potentials close to the equilibrium value for the M-Fc/M-Fc⁺ couple confined to the HOPG surface, Figure 9. At a substrate

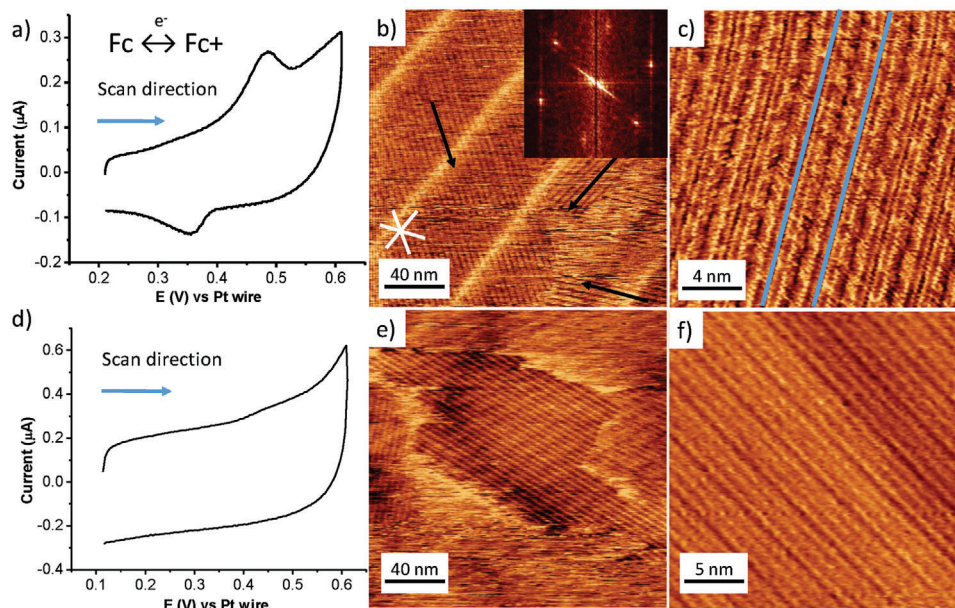


Figure 7. CVs of a) M-Fc/HOPG and d) M/HOPG in 0.1 M HClO₄ in the EC-STM cell. Scan rate, 50 mV s⁻¹. CE, RE: Pt wire. EC-STM images of b,c) M-Fc/HOPG (inset: FFT) and e,f) M/HOPG at a substrate potential of 0.1 V versus Pt. Tunneling parameters b,c) $V_{\text{bias}} = 0.9$ V, $I_t = 0.16$ nA; e,f) $V_{\text{bias}} = 1.24$ V, $I_t = 0.40$ nA.

potential of 0.3 V, partial oxidation of the M-Fc adlayer leads to pronounced dynamics, in which well-ordered islands are separated by disordered (presumably 2D gas-like) regions. The ordered islands are seen to change shape and size, as would be expected for a system close to equilibrium, and the large, isolated domain in Figure 9d may indicate 2D Ostwald ripening.^[19] Importantly, the disturbance caused by the tip during imaging may contribute to the observed dynamics. When the substrate potential is raised to 0.4 V, the ordered islands gradually disappear and only leave the disordered 2D gas, Figure 9e–h. Reversing the potential to 0.3 V, Figure 9i–l, causes ordered but continually changing islands to reappear. A further decrease of E_s to 0.2 V causes an almost complete crystallization of the adlayer, with only domain boundaries remaining blurry as molecules may occupy energetically closely matched positions that are also entropically favored, Figure 9m–p. At $E_s = 0.1$ V, finally, also the domain boundaries crystallize and become static, Figure 9q–t, restoring the starting situation. Control experiments with pedestal M/HOPG under the

same conditions did not reveal adlayer dynamics (see Figure S1, Supporting Information), providing further evidence that the dynamics found for M-Fc/HOPG under electrochemical conditions are indeed redox-driven.

The possibility of M-Fc⁺ desorbing from the interface can be excluded as all experiments with HOPG/M-Fc in an aqueous solution were carried out in an electrolyte that does not contain M-Fc, and all the electroactive material is initially confined at the interface. If oxidation of the redox species leads to desorption of M-Fc⁺ that subsequently diffuses away from the electrode, the redox signal would strongly decrease after the first cycle—behavior that we observed in earlier work.^[13] In the present case, the redox signal was stable on repeated cycling, allowing us to measure the scan rate dependence we show in Figure 6d–f. A further argument for the presence of the M-Fc⁺ adsorption gas is the reversibility of our EC-STM observations, where small changes in potential cause the visible increase or decrease of 2D crystal size (Figures 8 and 9). If one of the forms would desorb and diffuse

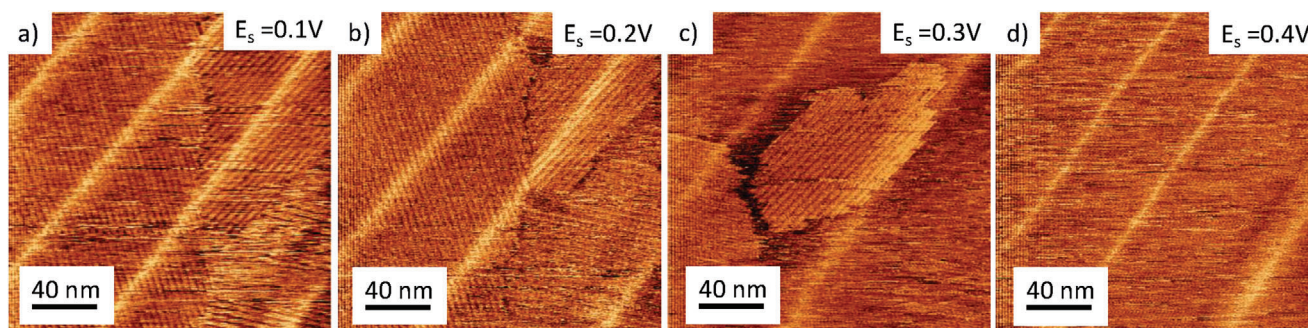


Figure 8. EC-STM images of M-Fc/HOPG in 0.1 M HClO₄ as a function of substrate potential E_s versus Pt as indicated. Tunneling parameters: a,b) $V_{\text{bias}} = 1.0$ V; c,d) $V_{\text{bias}} = 1.1$ V; a–d) $I_t = 0.16$ nA.

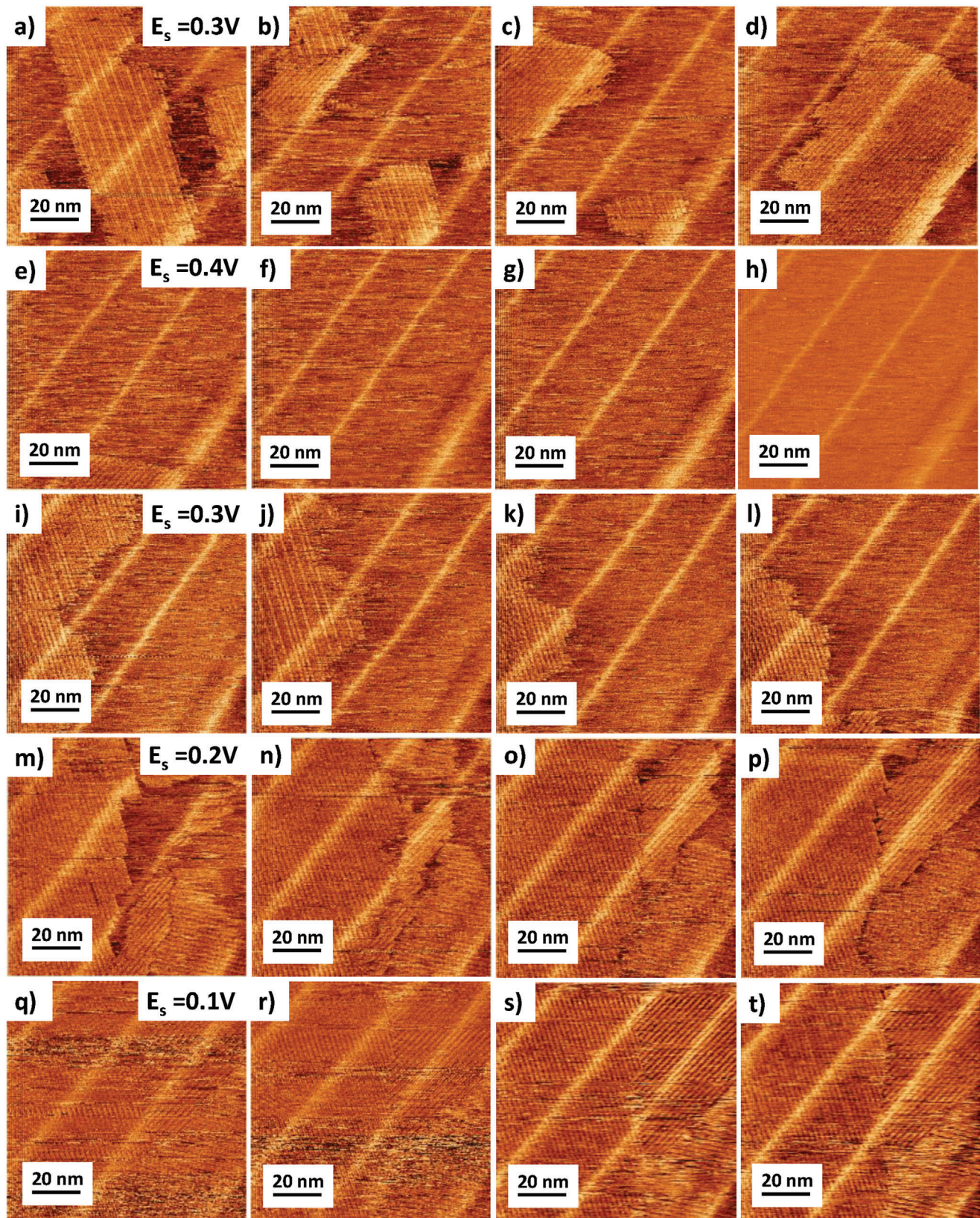


Figure 9. Adlayer dynamics of M-Fc/HOPG in 0.1 M HClO₄ as a function of substrate potential E_s versus Pt as indicated. Tunneling parameters: a–l) $V_{\text{bias}} = 1.1$ V; m–t) $V_{\text{bias}} = 1.0$ V; $I_t = 0.16$ nA for all images.

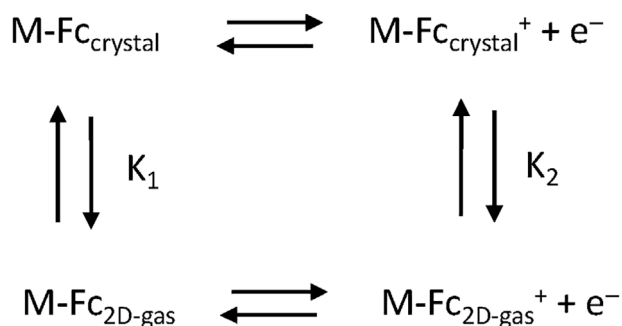


Figure 10. Square scheme mechanism to rationalize electrochemical and EC-STM behavior of M-Fc/HOPG in 0.1 M aqueous perchlorate.

away from the interface, especially enhanced by active scanning with the tip, the growth of the 2D crystals at more negative potentials could not be explained on the timescale of the experiment. Finally, from the structure of the molecule, Figure 1, with extended alkyl chains and no hydrophilic functional groups, we do not expect a single ferrocenium group in M-Fc⁺ to be sufficient to solubilize this large hydrophobic molecule in aqueous solution.

As we now have strong microscopic evidence for both redox-driven phase transitions and observable dynamics in M-Fc adlayers, clearly linked to the presence of the ferrocene group, we return to discussing the electrochemical behavior and the mechanism of the redox switching. In particular, the experimentally observed asymmetry between the oxidation and reduction peaks, Figure 6d, can be explained by a “square scheme” mechanism in which M-Fc exists in two forms, the crystalline form (M-Fc_{crystal}) and the 2D adsorption gas form (M-Fc_{2D-gas}), Figure 10. Each of these forms behaves as a separate redox couple with its own E^0 , described by the horizontal arrows in the scheme. In addition, both the reduced and the oxidized form of M-Fc are part of chemical equilibria between crystal and 2D gas, described by the vertical arrows in the scheme. By assuming that the equilibrium favors the crystalline form for neutral M-Fc, and the 2D adsorption gas form for oxidized M-Fc⁺, it is straightforward to reproduce the experimentally observed asymmetry in the cyclic voltammograms by simulation of the square scheme mechanism using the KISSA 1D software (see Figure S2, Supporting Information).^[20] Importantly, these assumptions are in full compliance with our EC-STM observations of the reduced and oxidized forms of the layer.

To further demonstrate the considerable potential of cyclophanes toward 3D supramolecular architectures, we performed the following host-guest experiment. In recent work, we described a selective and highly sensitive sensor surface based on β -cyclodextrin, a host molecule that forms inclusion complexes with hydrophobic guests of suitable size.^[21a] In that paper, we demonstrated selective electrochemical detection of ferrocene—the unit here tethered to the cyclophane—against a hundredfold higher background of hexacyanoferrate as a hydrophilic analyte that remained undetected. Here, we demonstrate the potential of using β -cyclodextrin as a structural complement with strong affinity and suitable size for Fc. Figure 11a shows an ordered M-Fc/HOPG adlayer as visualized by EC-STM. After adding 10 μ M β -cyclodextrin to the electrolyte, imaging was resumed and resulted in Figure 11b. Bright protrusions appear on the surface, indicated by circles, likely indicating the successful formation of the Fc- β -cyclodextrin inclusion complex, and confirming the viability of this supramolecular strategy for 3D nanoarchitecture design. As the stability constant of the inclusion complex between neutral ferrocene and β -cyclodextrin is 4100 ± 200 L mol⁻¹ in aqueous solution,^[21b] there is a large thermodynamic driving force for quantitative formation of this inclusion complex. Considering the physical dimensions of β -cyclodextrin (1.54 nm diameter at its widest point), its conical shape, and the closest spacing of the ferrocene units in the M-Fc layer (determined as $b = 2.14 \pm 0.2$ nm, see Figure 2d), a sufficiently long exposure of the M-Fc monolayer to the β -cyclodextrin solution is expected to lead to complete, if crowded, complexation of the ferrocene units. Further, in view of the large stability constant of the inclusion complex, the hydrophobic nature of the neutral M-Fc layer, and the hydrophilic exterior of β -cyclodextrin, we can confidently exclude nonspecific β -cyclodextrin adsorption in the present case.

Finally, we explore whether resonant tunneling, mediated by the Fc redox center, can be probed by electrochemical scanning tunneling spectroscopy (EC-STs), further expanding the device potential of cyclophanes that are fully integrated into advanced nanoarchitectures.^[22] Figure 12a shows a typical I-V curve for M-Fc molecular junctions in constant sample bias mode with $V_{\text{bias}} = 1.10$ V and $I_0 = 0.21$ nA. In this experiment, the bias voltage between tip and substrate is kept constant. The EC-STs measurements were started at a substrate potential of 0.1 V, where the Fc moiety is in its neutral state and the M-Fc adlayer is stable. Afterward, both the substrate and tip potentials are swept toward values more positive than the equilibrium potential E^0 with

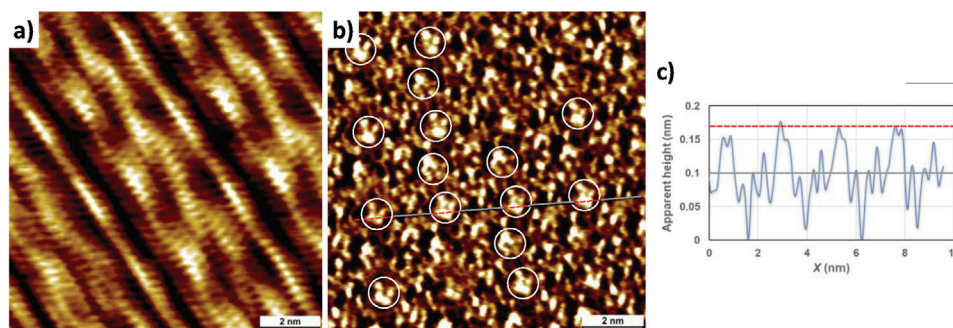


Figure 11. EC-STM images of M-Fc/HOPG in 0.1 M HClO₄ a) in the absence and b) in the presence of 10 μ M beta-cyclodextrin, at a substrate potential $E_s = 0.2$ V versus Pt. c) Line profile along the line in panel (b). Tunneling parameters: a,b) $V_{\text{bias}} = 1.1$ V, a) $I_t = 0.41$ nA; b) $I_t = 0.28$ nA.

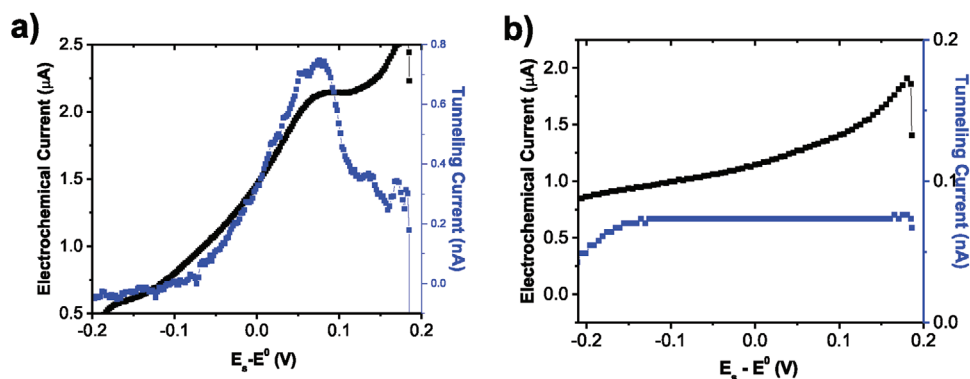


Figure 12. Linear sweep voltammogram (black trace) and EC-scanning tunneling spectrum (blue trace) of M-Fc/HOPG a) and M/HOPG b) in 0.1 M HClO_4 . Scan rate, 0.5 V/s. EC-STs measurements were recorded in constant bias mode with a) $V_{\text{bias}} = 1.10$ V, $I_0 = 0.21$ nA and b) $V_{\text{bias}} = 1.15$ V, $I_0 = 0.18$ nA. The potential range is centered around the formal potential of M-Fc. The tunneling current was background-corrected by subtracting the initial setpoint current.

a constant rate. Figure 12a, blue trace shows a clear resonance in the tunneling current that correlates with the oxidation feature in the linear sweep voltammogram, black trace. For ease of comparison, the STS curve is shown as a function of overpotential $\eta = E_s - E^0$ (i.e., the difference between applied and formal potential for M-Fc). The tunneling current is asymmetric around $\eta = 0$ V, with a higher value at $\eta > 0$ than that at $\eta < 0$, which suggests a higher conductance of M-Fc in its oxidized form than its neutral form.^[8–9] The blank experiment with the pedestal-only M/HOPG adlayer shows no tunneling junction effect in the same potential range, Figure 12b.

3. Conclusion

Since their initial synthesis in 1949, cyclophanes have come a long way toward versatile and powerful building blocks for novel smart materials. In this paper, we have demonstrated the electrochemical switching of supramolecular 2D structure in a 3D ferrocene-functionalized cyclophane. The redox-driven transition between an ordered 2D crystal and a highly mobile 2D adsorption gas was demonstrated using electrochemical STM and rationalized based on a “square scheme” mechanism that explains experimentally observed pronounced asymmetry in cyclic voltammetry. Toward further development of cyclophanes as multifunctional parts in a “supramolecular toolbox”, we have also demonstrated that i) functionalization of the pedestal can be orthogonal to structural and functional behavior, as evidenced by random mixing of tectons at the molecular level; ii) additional supramolecular principles and binding motifs can be exploited to achieve further levels of complexity, as evidenced by forming host–guest complexes between M-Fc and β -cyclodextrin; iii) sophisticated electronic and other functions can be successfully built into cyclophane-based nanoarchitectures, as evidenced by device-like behavior in M-Fc/HOPG molecular junctions when probed by electrochemical scanning tunneling spectroscopy.

4. Experimental Section

All STM experiments were performed using an Agilent SPM system in constant-current mode. The ambient STM tips were produced by mechan-

ically cutting Pt/Ir wire (80%/20%, diameter 0.25 mm). For EC-STM, W tips were etched electrochemically in 2 M KOH and coated with hot glue to minimize Faradaic current. The bias voltage refers to the substrate. AFM measurements were performed in air with a Multimode AFM with a Nanoscope IV controller (Veeco/Digital Instruments) in tapping mode. HOPG substrates (grade ZYB) were obtained from Advanced Ceramics Inc., Cleveland, USA. STM and AFM data analysis was performed using Scanning Probe Image Processor (SPIP) software (Image Metrology ApS).

Ultrapure water (Milli-Q, Millipore, 18.2 M Ω cm, total organic carbon <3 ppb) was used throughout. Reagent grade perchloric acid and sodium perchlorate were purchased from Merck and Sigma–Aldrich, respectively, and used without further purification. Electrolyte solutions were deoxygenated with argon (grade 5.0, Praxair) before use. M and M-Fc were synthesized according to published procedures.^[7,8] These molecules were dissolved in 1-phenyloctane (98%, Sigma–Aldrich) separately or mixed for ambient STM at the solid-liquid interface. Dry films of M and M-Fc on HOPG were prepared by dropcasting 20 μL of a 100-fold diluted saturated solution in ethanol (spectroscopic grade, Sigma–Aldrich), followed by slow evaporation of the solvent in a sealed petri dish. For cyclic voltammetry, M and M-Fc were dissolved in dichloromethane (DCM, 99.8%, Sigma–Aldrich) containing 0.1 M tetrabutylammonium hexafluorophosphate (Bu_4NPF_6 , 99%, Sigma–Aldrich) as supporting electrolyte. All electrochemical measurements were performed using an Autolab PGSTAT101 potentiostat (Metrohm-Autolab BV, The Netherlands). The HOPG surface was freshly cleaved using Scotch tape prior to each experiment. Voltammetry was performed in a lab-built single-compartment three-electrode cell, with HOPG as working electrode (geometric area 38.5 mm²), Pt wire counter, and Ag/AgCl/3 M NaCl reference electrodes.

Supporting Information

Supporting Information is available from the Wiley Online Library or from the author.

Acknowledgements

This work was supported by Research Foundation – Flanders (FWO) (GF9118N, G0H2122N) under the Excellence of Science EOS program (project 30489208, 40007495), Funds KU Leuven (C14/23/090). SFLM acknowledges support from the Austrian Science Fund (FWF, project I3256-N36), Lancaster University, and Materials Science Lancaster.

Conflict of Interest

The authors declare no conflict of interest.

Data Availability Statement

The data that support the findings of this study are available in the supplementary material of this article.

Keywords

cyclophanes, electrochemical switching, graphite, scanning tunneling microscopy, supramolecular self-assembly

Received: December 12, 2023
Revised: March 15, 2024
Published online:

- [1] C. Brown, A. J. N. Farthing, *Nature*. **1949**, 164, 915.
[2] D. J. Cram, H. Steinberg, *J. Am. Chem. Soc.* **1951**, 73, 5691.
[3] a) M. S. Collins, M. E. Carnes, B. P. Nell, L. N. Zakharov, D. W. Johnson, *Nat. Commun.* **2016**, 7, 11052; b) P. G. Ghasemabadi, T. Yao, G. Bodwell, *Chem. Soc. Rev.* **2015**, 44, 6494.
[4] a) D. C. Braddock, I. D. MacGilp, B. G. Perry, *J. Org. Chem.* **2002**, 67, 8679; b) L. Han, Y. Lei, P. Xing, X.-L. Zhao, B. J. Jiang, *J. Org. Chem.* **2015**, 80, 3752.
[5] a) J. Zyss, I. Ledoux, S. Volkov, V. Chernyak, S. Mukamel, G. P. Bartholomew, G. C. Bazan, *J. Am. Chem. Soc.* **2000**, 122, 11956; b) S. T. Schneebeli, M. Kamenetska, Z. Cheng, R. Skouta, R. A. Friesner, L. Venkataraman, R. J. Breslow, *J. Am. Chem. Soc.* **2011**, 133, 2136; c) A. H. David, A. Garci, S. Abid, X. Li, R. M. Young, J. S. Seale, J. E. Hornick, C. S. Azad, Y. Jiao, I. J. Roy, *J. Am. Chem. Soc.* **2023**, 145, 9182; d) D. S. Seferos, A. S. Blum, J. G. Kushmerick, G. C. Bazan, *J. Am. Chem. Soc.* **2006**, 128, 11260; e) W. J. Oldham, Y.-J. Miao, R. J. Lachicotte, G. C. Bazan, *J. Am. Chem. Soc.* **1998**, 120, 419; f) G. P. Bartholomew, I. Ledoux, S. Mukamel, G. C. Bazan, J. J. Zyss, *J. Am. Chem. Soc.* **2002**, 124, 13480. g) I. Roy, A. H. David, P. J. Das, J. P. David, J. F. Stoddart, *Chem. Soc. Rev.* **2022**, 51, 5557.
[6] K. Cai, M. C. Lipke, Z. Liu, J. Nelson, T. Cheng, Y. Shi, C. Cheng, D. Shen, J.-M. Han, S. J. Vemuri, Y. Feng, C. L. Stern, W. A. Goddard iii, M. R. Wasielewski, J. F. Stoddart, *Nat. Commun.* **2018**, 9, 5275.
[7] a) M. D. Watson, F. Jäckel, N. Severin, J. P. Rabe, K. J. Müllen, *J. Am. Chem. Soc.* **2004**, 126, 1402; b) F. Matino, G. Schull, F. Köhler, S. Gabutti, M. Mayor, R. J. Berndt, *Proc Natl Acad Sci.* **2011**, 108, 961; c) N. Schneider, F. Matino, G. Schull, S. Gabutti, M. Mayor, R. J. Berndt, *Phys. Rev. B.* **2011**, 84, 153403; d) K. Scheil, N. Lorente, M.-L. Bocquet, P. C. Hess, M. Mayor, R. J. Berndt, *J. Phys. Chem. C.* **2017**, 121, 25303; e) M. Metzelaars, S. Schleicher, T. Hattori, B. Borca, F. Matthes, S. Sanz, D. E. Bürgler, J. Rawson, C. M. Schneider, P. J. Kögerler, *Chem. Sci.* **2021**, 12, 8430.
[8] S. Gabutti, M. Knutzen, M. Neuburger, G. Schull, R. Berndt, M. J. Mayor, *Chem. Commun.* **2008**, 44, 2370.
[9] a) D. Bléger, D. Kreher, F. Mathevet, A. J. Attias, I. Arfaoui, G. Metgé, L. Douillard, C. Fiorini-Debuisschert, F. Charra, *Angew. Chem., Int. Ed.* **2008**, 47, 8412; b) D. Bléger, F. Mathevet, D. Kreher, A. J. Attias, A. Bocheux, S. Latil, L. Douillard, C. Fiorini-Debuisschert, F. Charra, *Angew. Chem., Int. Ed.* **2011**, 50, 6562; c) P. Du, M. Jaouen, A. Bocheux, C. Bourgogne, Z. Han, V. Bouchiat, D. Kreher, F. Mathevet, C. Fiorini-Debuisschert, F. Charra, *Angew. Chem., Int. Ed.* **2014**, 126, 10224; d) P. Du, D. Kreher, F. Mathevet, P. Maldivi, F. Charra, A. J. Attias, *ChemPhysChem.* **2015**, 16, 3774; e) S. Le Liepvre, P. Du, D. Kreher, F. Mathevet, A.-J. Attias, C. Fiorini-Debuisschert, L. Douillard, F. Charra, *ACS Photonics.* **2016**, 3, 2291.
[10] a) W. R. Browne, B. L. Feringa, *Annu. Rev. Phys. Chem.* **2009**, 60, 407; b) H. Zhou, C. C. Mayorga-Martinez, S. Pané, L. Zhang, M. Pumera, *Chem. Rev.* **2021**, 121, 4999.
[11] B. Schnyder, D. Alliata, R. Kötz, H. J. Siegenthaler, *Appl. Surf. Sci.* **2001**, 173, 221.
[12] a) J.-M. Savéant, *Elements of Molecular and Biomolecular Electrochemistry: An Electrochemical Approach to Electron Transfer Chemistry*, John Wiley & Sons, Hoboken, New Jersey **2006**; b) S. F. L. Mertens, G. Mészáros, T. Wandlowski, *Phys. Chem. Chem. Phys.* **2010**, 12, 5417.
[13] X. Guégano, A. L. Kanibolotsky, C. Blum, S. F. L. Mertens, S. X. Liu, A. Neels, H. Hagemann, P. J. Skabara, S. Leutwyler, T. Wandlowski, A. Hauser, S. Decurtins, *Chem. Eur. J.* **2009**, 15, 63.
[14] D. R. Lide, *CRC Handbook of Chemistry and Physics*, Vol. 85, CRC press, Florida, United States **2004**.
[15] a) K. Cui, K. S. Mali, O. Ivashenko, D. Wu, X. Feng, M. Walter, K. Müllen, S. De Feyter, S. F. L. Mertens, *Angew. Chem., Int. Ed.* **2014**, 53, 12951; b) S. Sadegh Hassani, Y.-G. Kim, E. J. L. Borguet, *Angew. Chem., Int. Ed.* **2011**, 27, 14828; c) K. Cui, O. Ivashenko, K. S. Mali, D. Wu, X. Feng, M. Walter, K. Müllen, S. De Feyter, S. F. L. Mertens, *Chem. Commun.* **2014**, 50, 10376; d) T. M. T. Huynh, T. H. Phan, O. Ivashenko, S. F. L. Mertens, S. De Feyter, *Nanoscale.* **2017**, 9, 362.
[16] a) S. F. L. Mertens, *Surface Science and Electrochemistry* (Ed.: K. Wandelt), 4, Elsevier, Amsterdam **2018**, pp. 13–23; b) K. Cui, I. Dorner, S. F. L. Mertens, *Curr. Opin. Electrochem.* **2018**, 8, 156; c) K. Cui, K. S. Mali, D. Wu, X. Feng, K. Müllen, M. Walter, S. De Feyter, S. F. L. Mertens, *Angew. Chem., Int. Ed.* **2020**, 59, 14049.
[17] a) T. Sagara, K. Miuchi, *J. Electroanal. Chem.* **2004**, 567, 193; b) T. Higashi, Y. Shigemitsu, T. Sagara, *Langmuir.* **2011**, 27, 13910.
[18] R. Wen, B. Rahn, O. M. Magnussen, *J. Phys. Chem. C.* **2016**, 120, 15765.
[19] a) O. Krichevsky, J. Stavans, *Phys. Rev. E.* **1995**, 52, 1818; b) T. K. Piskorz, A. H. de Vries, S. De Feyter, J. H. van Esch, *J. Phys. Chem. C.* **2018**, 122, 24380.
[20] C. Amatore, O. Klymenko, I. Svir, *Electrochem. Commun.* **2010**, 12, 1170.
[21] a) Z. Li, J. F. Van Guyse, V. R. de la Rosa, H. Van Gorp, P. Walke, M. C. Rodríguez González, H. Uji-i, R. Hoogenboom, S. De Feyter, S. F. L. Mertens, *Adv. Funct. Mater.* **2019**, 29, 1901488; b) D. Osella, A. Carretta, C. Nervi, M. Ravera, R. Gobetto, *Organometallics.* **2000**, 19, 2791.
[22] a) I. Díez-Pérez, Z. Li, S. Guo, C. Madden, H. Huang, Y. Che, X. Yang, L. Zang, N. Tao, *ACS Nano.* **2012**, 6, 7044; b) A. C. Aragonès, N. Darwish, S. Ciampi, L. Jiang, R. Roesch, E. Ruiz, C. A. Nijhuis, I. Díez-Pérez, *J. Am. Chem. Soc.* **2019**, 141, 240; c) R. Nichols, *Electrochim. Acta.* **2021**, 387, 138497; d) T. Albrecht, A. Guckian, A. M. Kuznetsov, J. G. Vos, J. Ulstrup, *J. Am. Chem. Soc.* **2006**, 128, 17132; e) T. Albrecht, S. F. L. Mertens, J. Ulstrup, *J. Am. Chem. Soc.* **2007**, 129, 9162.